A new EGFR and c-Met bispecific NIR-II fluorescent probe for visualising colorectal cancer and metastatic lymph nodes

Shangkun Jin,[a,b,c,k] Changjian Li,[d,e,k] Xiaohua Jia,[c,f,h] Jichuan Quan,[a] Xiaoyong Guo,[g] Wenzhi Kong,[h] Yueqi Wang,[c] Yuhan Wang,[a] Jie Tian,[c,d,e,i,***] Zhenhua Hu,[c,i,j,**] and Jianqiang Tang[a,*]

[a]Department of Colorectal Surgery, National Cancer Center/National Clinical Research Center for Cancer/Cancer Hospital, Chinese Academy of Medical Sciences and Peking Union Medical College, Beijing, 100021, PR China
[b]Department of Colorectal Surgery, Clinical Oncology School of Fujian Medical University, Fujian Cancer Hospital, Fuzhou, 350004, Fujian, PR China
[c]Key Laboratory of Molecular Imaging of Chinese Academy of Sciences, Institute of Automation, Chinese Academy of Sciences, Beijing, 100190, PR China
[d]School of Engineering Medicine, Beihang University, Beijing, 100191, PR China
[e]Key Laboratory of Big Data-Based Precision Medicine (Beihang University), Ministry of Industry and Information Technology, Beijing, 100191, PR China
[f]Department of Radiology, Beijing Youan Hospital Capital Medical University, Beijing, 100069, PR China
[g]Key Laboratory of Carcinogenesis and Translational Research (Ministry of Education), Department of Gastrointestinal Cancer Center, Ward I, Peking University Cancer Hospital & Institute, Beijing, PR China
[h]Department of Gynecologic Oncology, Beijing Obstetrics and Gynecology Hospital, Capital Medical University. Beijing Maternal and Child Health Care Hospital, Beijing, 100006, PR China
[i]School of Artificial Intelligence, University of Chinese Academy of Sciences, Beijing, 100049, PR China
[j]National Key Laboratory of Kidney Diseases, Beijing, 100853, PR China

eBioMedicine
2025;115: 105687
Published Online xxx
https://doi.org/10.1016/j.ebiom.2025.105687

Summary

Background The aim of the study was to increase the specificity and targeting of tumour imaging, targeting molecules that enable the simultaneous recognition and binding of multiple tumour-associated receptors. We constructed a NIR-II fluorescence probe based on a bispecific antibody to epidermal growth factor receptor (EGFR) and cellular mesenchymal–epithelial transition factor (c-Met) for visualising colorectal cancers (CRCs) and metastatic lymph nodes.

Methods The expression of EGFR and c-Met in tumour and metastatic lymph node specimens from patients with CRC was examined using immunohistochemistry. The EGFR and c-Met bispecific antibody (Rybrevant) was labelled, and its cell-specific binding ability was assessed using laser confocal microscopy. Subcutaneous CRC and orthotopic tumour models were constructed to evaluate the fluorescence imaging of the probe *in vivo*. To assess the performance of Rybrevant-IRDye800CW in the differential diagnosis of metastatic lymph nodes, a CRC lymph node metastasis model was constructed using human CRC cells implanted in mouse claw pads. Finally, surgically resected CRC tumours and lymph node specimens were incubated with Rybrevant-IRDye800CW for fluorescence NIR-II imaging to evaluate the efficacy of Rybrevant-IRDye800CW for preclinical visualisation.

Findings The combined expression rate of EGFR and c-Met in CRC and metastatic lymph nodes was significantly higher than the single-target expression rate. The bispecific probe Rybrevant-IRDye800CW was successfully synthesised, and its fluorescence signal could be extended up to 1600 nm using NIR-II imaging. Cell incubation experiments showed that the fluorescence intensity of Rybrevant-IRDye800CW was strongly correlated with EGFR and c-Met overexpression of the cells. NIR-II *in vivo* fluorescence imaging showed that double-positively expressing subcutaneous tumours significantly uptook Rybrevant-IRDye800CW after tail vein injection of the probe, which rapidly accumulated within the tumours in about 6 h. In EGFR and or c-Met blockade assays, subcutaneous tumours showed weaker uptake of Rybrevant-IRDye800CW. Similarly, Rybrevant-IRDye800CW was specifically identified in orthotopic CRC and lymph node metastasis models, with all orthotopic tumours showing

*Corresponding author. Department of Colorectal Surgery, National Cancer Center/National Clinical Research Center for Cancer/Cancer Hospital, Chinese Academy of Medical Sciences and Peking Union Medical College, Beijing, 100021, PR China.
**Corresponding author. Key Laboratory of Molecular Imaging of Chinese Academy of Sciences, Institute of Automation, Chinese Academy of Sciences, No. 95 Zhongguancun East Road, Hai Dian District, Beijing, 100190, PR China.
***Corresponding author. Key Laboratory of Molecular Imaging of Chinese Academy of Sciences, Institute of Automation, Chinese Academy of Sciences, No. 95 Zhongguancun East Road, Hai Dian District, Beijing, 100190, PR China.
E-mail addresses: tangjq@cicams.ac.cn (J. Tang), zhenhua.hu@ia.ac.cn (Z. Hu), jie.tian@ia.ac.cn (J. Tian).
[k]These authors contributed equally to this work.

high tumour-to-background ratios in NIR-II imaging. In a NIR-II preclinical study, Rybrevant-IRDye800CW could specifically identify fresh human CRC and its metastatic lymph node tissue.

Interpretation This study confirmed the complementary EGFR and c-Met expression in CRC and its metastatic lymph nodes. Compared to single-target probes, EGFR and c-Met dual-specific fluorescent probes identified CRC and its metastatic lymph nodes using NIR-II imaging. Thus, NIR-II-guided R0 surgery was performed to resect the CRC and metastatic lymph nodes.

Fundings This study was supported by the Beijing Natural Science Foundation (Grant numbers: L222054, 7244517, 4232058, L248026, L232020), National Natural Science Foundation of China (NSFC) (92059207, 92359301, 92259303, 62027901, 81930053, 81227901, U21A20386), CAS Youth Interdisciplinary Team (JCTD-2021-08), and the Fundamental Research Funds for the Central Universities (Grant no. JK2024-2-35-02).

Keywords: CRC; Metastatic lymph nodes; Bispecific antibody; NIR-II; Fluorescence imaging

Research in context

Evidence before this study

For patients with colorectal cancer, resection of the tumour and its metastatic lymph nodes is extremely important; however, there are difficulties in accurately identifying and completely removing colorectal cancer and its metastatic lymph nodes intraoperatively. Second near-infrared window (NIR-II, 1000–1700 nm) fluorescence imaging is a novel imaging technique that can compensate for the insufficient penetration depth, low resolution, and low background of NIR-I. It has been validated in clinical trials and is a powerful tool for real-time surgical imaging. For colorectal cancer, metastatic lymph node clearance is difficult, and the leftover metastatic lymph nodes seriously affect the health and safety of patients. However, studies using NIR-II fluorescence imaging for the intraoperative navigation of metastatic lymph nodes in colorectal cancer are lacking.

Added value of this study

In this study, we designed and synthesised a bispecific NIR-II-targeted fluorescent probe, Rybrevant-IRDye800CW, which specifically recognised EGFR and c-Met-positive colorectal cancer and its metastatic lymph nodes. We validated the effectiveness of the probe at the cellular level, in animal models, and in patient tumour specimens.

Implications of all the available evidence

In this study, we developed a dual-targeted NIR-II fluorescent probe for detecting colorectal cancer and metastatic lymph nodes, aiding surgeons in accurate intraoperative imaging and resection, reducing residual tumours, and providing evidence for future clinical applications.

Introduction

Colorectal cancer (CRC) is a tumour that ranks third and second for morbidity and mortality worldwide, respectively, making it a serious threat to human lives and health.[1–3] Initial progress has been made in recent years in molecular targeted therapy and immunotherapy; however, the five-year survival rate of metastatic CRC is still only 10%.[4] Complete tumour resection (R0) can significantly improve the overall survival rate and reduce the recurrence rate. However, it is closely associated with positive tumour margins, which occur in 5% of cases after CRC surgery. The recurrence rate of CRC increases with the tumour stage, reaching as high as 14% in T4 CRC.[5] In addition, patients with locally progressive and recurrent rectal cancer have a higher rate of positive margins.[6,7] Lymph node metastasis is the most common route of metastasis in CRC and is the main factor for metastatic recurrence after R0 resection; some patients with lymph node-negative CRC also experience recurrence after surgery.[8] Surgeons can rely only on visual and tactile information during surgery; therefore, it is difficult to distinguish between fibrosis and tumour lesions accurately, and it is impossible to maximise the resection of tumour tissues and metastatic lesions to improve patient prognosis.

Fluorescence imaging technology used for the precise clinical resection of tumours has further improved the accuracy of complete CRC resection.[9,10] For example, fluorescence-guided surgery (FGS) assists surgeons in performing complete tumour resection by enhancing their ability to detect tumours.[11] Near-infrared fluorescence imaging (NIR-FI) is a real-time imaging technique that combines NIRFI-targeted probes with a fluorescence imaging system to identify specific molecular targets in tumour tissues and to differentiate between tumour and normal tissues.[12] Currently,

indocyanine green (ICG) is the only optical probe approved by the U.S. Food and Drug Administration for use in CRC surgery, enabling the diagnosis and monitoring of tumours and their lymph nodes. ICG can visualise lymphatic vessels and lymph nodes; however, pathology has shown that ICG molecules are found in non-tumourigenic areas of metastatic lymph nodes, which do not show metastatic areas, indicating that ICG lacks specificity.[13] Therefore, new fluorescent imaging probes for primary CRC tumours and metastatic lymph nodes are urgently required to improve the success of CRC surgery.

Some targets have already been developed for molecular imaging applications in clinical CRC diagnosis,[14–18] such as epidermal growth factor receptor (EGFR) and cellular mesenchymal–epithelial transition factor (c-Met), which have been widely investigated for tumour-targeted fluorescence molecular imaging applications because of their high expression in tumours. However, owing to the heterogeneity of tumour cell expression, a single target often fails to cover most tumours, resulting in low sensitivity of tumour imaging.[19] In CRC, EGFR is overexpressed in 60–80% of patients,[20,21] whereas c-Met overexpression occurs in 50–70%.[22–24] One possible approach for increasing the specificity and targeting of imaging is to target molecules that simultaneously recognise and bind to multiple tumour-associated receptors. Bispecific antibodies have attracted significant attention in diagnosing and treating tumours, and an increasing number of molecular imaging studies of multi-target combinations have been validated in preclinical settings.[19,25,26] Rybrevant (Amivantamab, JNJ-61186372) is a new bispecific antibody demonstrated to be safe in clinical trials and can target both EGFR and c-Met on the tumour surface.[27] The ability of Rybrevant to target different markers may bypass the limitations of single-targeted antibodies, leading to speculation about its superior application in imaging CRC and its metastatic lesions.

Light in the NIR-II band (1000–1700 nm) is less absorbed in biological tissues than that in the NIR-I (700–900 nm), providing deeper tissue penetration (20 mm) and better tumour imaging.[28] NIR-II in the development of a variety of NIR-II fluorescent probes, such as quantum dots, single-walled carbon nanotubes, organic dyes, etc. Since safety is not widely used in human. IRDye800CW dye is an amine-responsive, near-infrared, highly water-soluble fluorescent dye that is widely used for NIR-I window-targeted imaging of labelled proteins and antibodies. The tail emission of ICG can be used to perform NIR-II imaging, which is superior to NIR-I.[29–31] Reports of the application of NIR-II in CRC surgery are limited,[32] and, to our knowledge, the use of bispecific fluorescent probes to identify and diagnose NIR-II-targeted CRC and its metastatic lymph nodes has not been reported. Therefore, we constructed a targeted NIR-II probe by combining Rybrevant, a bispecific anti-EGFR and c-Met monoclonal antibody, with the near-infrared fluorescent dye IRDye800CW to investigate the value of NIR-II fluorescence imaging for preclinical studies in the intraoperative navigation of CRC and its metastatic lymph nodes (Fig. 1).

Methods

Ethical statement

This study was approved by the Medical Ethics Review Panel of the Cancer Hospital of the Chinese Academy of Medical Sciences (Ethics no. 22/248-3450). Informed consent was obtained from all participants. All animal experiments were conducted according to the principles of the Declaration of Helsinki. All animal experiments in this study were approved by Ethics Committee of Institute of Automation, Chinese Academy of Sciences (CASIA Issue No. IA21-2302-420303).

Immunohistochemical staining (IHC)

Fresh tissues were fixed with formaldehyde, washed with phosphate buffer (PBS), dehydrated with ethanol, and soaked in distilled water. EDTA pH 8.0 (G1207-1L, Servicebio, Wuhan, China) was placed in boiling water, and paddles were placed on the sectioning frame, pressurised sufficiently, and cooled to room temperature. The samples were washed in PBS, and 3% hydrogen peroxide (H2O2) in 80% methanol was added dropwise onto the tissue microarrays for 10 min. After successive treatments with H2O2 and 10% goat serum, the slices were incubated with Anti-EGFR Rabbit pAb (Servicebio Cat# GB111504-100, RRID:P00533) or anti-c-Met (Servicebio Cat# GB115048-100, RRID:P08581) antibodies for 1 h at room temperature. After rinsing, the sections were further incubated with secondary antibody (GB23303, Servicebio, Wuhan, China), stained with 3,3,-diaminobenzidine, diaminobenzidine, stained with haematoxylin, differentiated with ethanol hydrochloride, dehydrated, and sealed for microscopic imaging. High-resolution digital images were acquired with a Panorama 250 Flash II digital scanner (3DHISTECH, Budapest, Hungary). IHC staining was subsequently quantified using the ImageJ IHC profiler (National Institutes of Health), and EGFR and c-Met overexpression was defined as >50% staining.

Synthesis and characterisation of Rybrevant-IRDye800CW

The EGFR and c-Met bispecific antibody Amivantamab (Rybrevant, Janssen Pharmaceuticals, USA) (50 mg/ml) labelled the NIRF dye IRDye800CW NHS ester (LI-COR, Bioscience). IRDye800CW is a NIRF resin dye with a broad range of absorption (778 nm) and emission peaks (794 nm) that have a favourable biosafety profile.[33,34] Rybrevant-IRDye800CW was prepared by coupling Rybrevant with the IRDye800CW NIR resin dye using the synthesis of EGFR-IRDye800CW as described

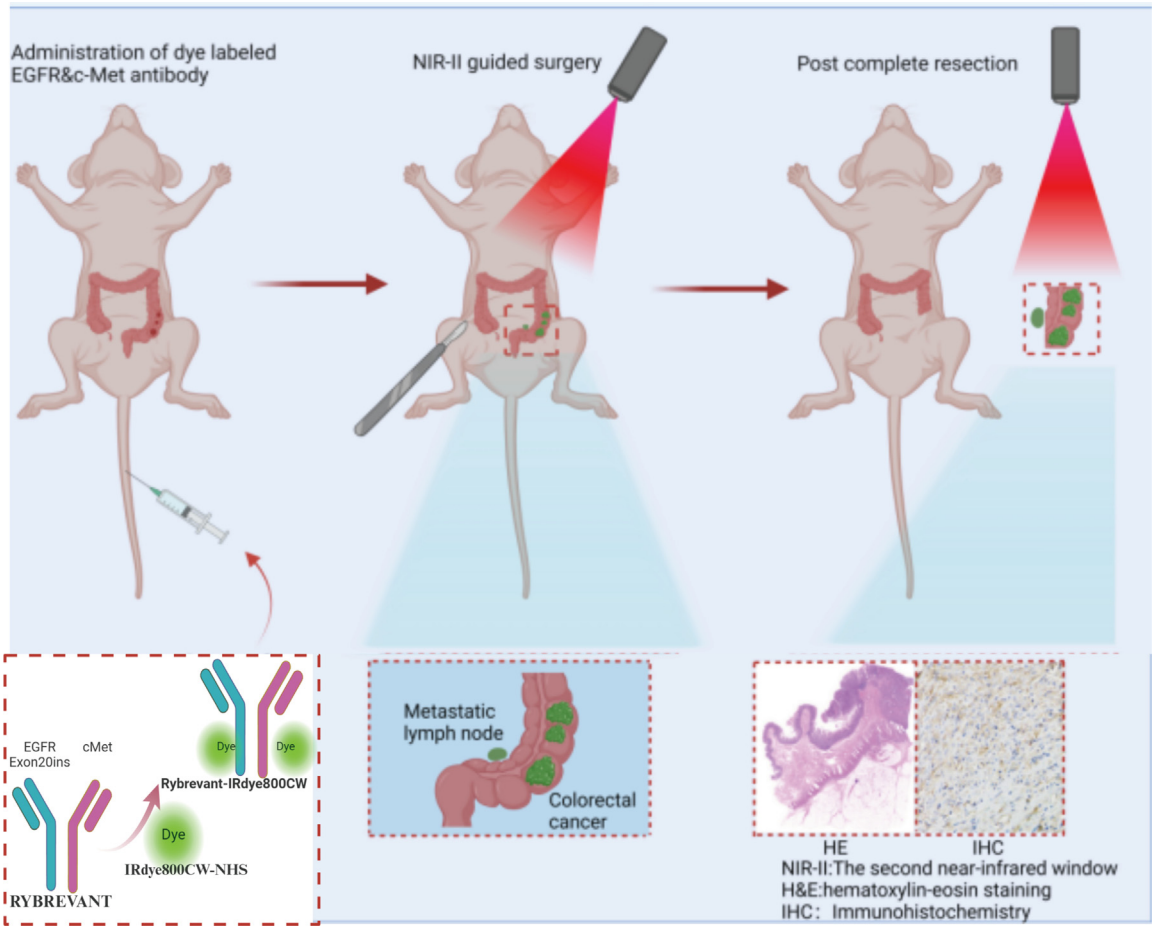

Fig. 1: The design and synthesis of fluorescent probes targeting EGFR and c-Met and the construction of an animal model for Colorectal cancer (CRC) and its metastatic lymph nodes. Tail vein injection of dual-targeted fluorescent probe Rybrevant-IRDye800CW and imaging on a dark-field NIR-II fluorescence imager. The excision of colorectal tumours and their metastatic lymph nodes under NIR-II fluorescence guidance and HE and IHC staining of subject specimens.

previously.[35] Briefly, the Rybrevant antibody was dissolved in phosphate solution at pH 8.5 and then a certain molar mass of IRDye800CW NHS was added. This mixture was stirred constantly at room temperature in the dark for 3 h before it was eluted and purified on a PD-10 column to remove the unreacted dye and obtain the purified probe.

NIR-I/II angiography

All animals were purchased from Beijing Huafukang Biological Science and Technology Co. Five-week-old Balb/c-nu male mice were administered 1–5 mg/kg Rybrevant-IRDye800CW via tail vein injection and the left hind limbs of the mice were subjected to angiography using a NIR-II camera (Xenics Cheetah-640CL TE3) with 1000, 1100, 1200, 1300, and 1400 nm filter slides. The samples were excited at 808 nm using an exposure time of 50 ms–1 s. NIR-I imaging was performed using a CMOS camera (PCO, Germany) with an 850 ± 40-nm filter attached to capture NIR-I fluorescence excited at 792 nm for 30 ms. After acquiring the images, the maximum cross-sectional fluorescence intensity was calculated for the vascular region of interest to quantify the contrast within the vascular region of interest for both NIR-I and NIR-II imaging.

Cell culture

The human CRC cell lines HT29 (RRID: CVCL_0320), HCT116 (RRID: CVCL_0291), SW480 (RRID: CVCL 0546), SW620 (RRID: CVCL_0547), and RKO (RRID: CVCL_0504) were gifted by the Department of Gastroenterology, Peking University First Hospital, and cultured in DMEM (G4515-500 ML, Servicebio, Wuhan, China) supplemented with 10% foetal bovine serum and 1% penicillin–streptomycin at 37 °C and 5% CO_2 in a cell culture incubator.

Western blotting

When the cells grew to a density of 80–90%, they were collected and lysed using RIPA lysis buffer (G2002-100 ML, Servicebio, Wuhan, China), and the protein concentration was determined using the BCA Protein assay kit (G2026-1000T, Servicebio, Wuhan, China). Protein samples were boiled at 95 °C for 10 min in a metal bath, and 20 μg total protein was separated using sodium dodecylsulphate polyacrylamide gel electrophoresis. After separation, proteins were transferred to a PVDF membrane and incubated at room temperature with rabbit c-Met (Servicebio Cat# GB115048-100, RRID:ab—P08581), EGFR (Servicebio Cat# GB111504-100, RRID:ab—P00533), or β-actin (GB12001-100, 1:1000, Servicebio, Wuhan, China) antibodies overnight at 4 °C. After washing the membranes with PBS, they were incubated with goat polyclonal anti-rabbit IgG-HRP (GB23303, 1:5000, Servicebio, Wuhan, China) and anti-mouse IgG-HRP (GB23301, 1:5000, Servicebio, Wuhan, China) secondary antibodies at room temperature for approximately 1 h. After washing with a membrane wash buffer (Tris-buffered saline and Tween), the protein bands were detected using enhanced chemiluminescence using a ChemiDoc XRS + imaging system. Protein expression grey values were quantified using ImageJ software.

In vitro targeting evaluation

Approximately 5×10^5/ml cells were homogeneously inoculated in 15-mm glass-bottomed confocal dishes containing complete medium and grown to 70–90% density. Then, 200 μl 0.01 mg/ml Rybrevant-IRDye800CW probe was added to the cells and incubated for 2 h in the dark, washed with PBS, fixed in 4% paraformaldehyde, and stained with 4′,6-diamidino-2-phenylindole (DAPI). The samples were stored away from light before they were observed with a laser confocal microscope (THUNDER Imager EM Cryo CLEM, Leica, Germany). In binding site blocking experiments, cells were incubated with anti-targeted EGFR (Cetuximab, Generously provided by Merck Lyon Pharma, Germany), c-Met (Savolitinib Tablets, Generously provided by Hutchison Whampoa China) and dual-targeted EGFR & c-Met drugs (Rybrevant, Generously provided by Janssen Biotech, Inc. USA) at 100-fold probe concentration, respectively. Then, samples were washed with PBS and incubated in 200 μl 0.01 mg/ml Rybrevant-IRDye800CW probe. Finally, cell nuclei were stained with DAPI and imaged.

Construction of animal model

Five-week-old mice were purchased from the Beijing Huafukang Biotechnology Co. Approximately 2×10^6 HCT116 or RKO cells were subcutaneously inoculated onto the right dorsal side of Balb/c-nu mice to promote CRC subcutaneous tumour development. Orthotopic colorectal tumours of the caecum were established by making a median incision in the abdomen of the mice and slowly injecting 4×10^5 HCT116 cells into the plasma membrane layer of the caecum with a 30 G disposable sterile insulin syringe (0.3 mm × 8 mm). To establish a lymph node metastasis model of CRC, approximately 2×10^6 HCT116 cells were subcutaneously inoculated into the footpads of the right lower limbs of Balb/c-nu mice.

NIR-I/II fluorescence imaging

After successfully constructing the tumour mouse model, 100 μg Rybrevant-IRDye800CW was injected via the tail vein. The blocking group was subjected to binding site blocking experiments by intravenously injecting **2** mg unlabelled Cetuximab, Savolitinib, and Rybrevant into the mice 24 h before the probe was administered. A high-resolution camera (Xenics Cheetah-640CL TE3) equipped with an InGaAs detector array, a camera lens (Spacecom VF50M SWIR) capable of NIR-II fluorescence imaging, and filters fixed to the front of the lens (1000, 1100, 1200, 1300, 1300, and 1400 nm) was used to capture NIR-II fluorescence. A wavelength of 808 nm at a power of 50 mW/cm^2 was used to excite the fluorophore for an exposure time of 300–1000 ms. A region of interest was drawn along the tumour edge to obtain the mean fluorescence intensity (MFI). The MFI in the tumour and adjacent normal tissues was used to calculate the tumour-to-background ratio (TBR), and the fluorescence intensity values were calculated using ImageJ software. After the *in vivo* experiments, the mice were euthanised and dissected for ex vivo imaging of the tumours and major organs.

Statistical analysis

The experimental data are expressed as mean ± standard deviation (mean ± SD). A t-test was used to compare the two groups. Multiple sets of data were compared and the data satisfied normal distribution and chi-square, using a one-way ANOVA. All graphical production and statistical analyses were performed using GraphPad Prism8 software. NIR fluorescent images and their immunohistochemical results were quantitatively analysed using ImageJ software and converted to pseudo-colour. $p < 0.05$ were considered to be significantly different, where *, **, ***, and **** represent $p < 0.05$, $p < 0.01$, $p < 0.001$, and $p < 0.0001$, respectively.

Role of the funding source

The sponsors of the study had no role in the study design, data collection, data analyses, data interpretation, manuscript writing, or the decision to submit the paper for publication.

Results

Expression of EGFR and c-Met expression in CRCs and metastatic lymph node tissues

Tumour and metastatic lymph node specimens from patients with CRC (18 cases) were collected

intraoperatively to examine EGFR and c-Met protein expression. Sixteen of the 18 patients with CRC had metastatic lymph nodes, and the IHC staining results for EGFR and c-Met in CRC and metastatic lymph nodes are shown in the graphs (Fig. 2a–c). However, Fig. 2a left, EGFR and c-Met are negatively expressed in tumour tissues of the same patient with CRC (–), in the middle EGFR and c-Met are weakly positively expressed in tumour tissues of the same patient with CRC (+) and on the right side, EGFR and c-Met in the same patient with CRC tumour tissue are positive (++). The left side of Fig. 2c indicates negative expression (–) of EGFR and c-Met in metastatic lymph nodes of the same patient with CRC, and the middle and right sides indicate positive expression (+) of EGFR and c-Met in metastatic lymph nodes of the same patient with CRC. The proportions of EGFR expression, c-Met expression, both EGFR and c-Met expression, and either of the two (EGFR or c-Met) in CRCs were 72.2%, 66.7%, 50%, 88.9%, respectively (Fig. 2b), indicating that the overexpression rate of either protein was higher when the two proteins were combined. In CRC metastatic lymph nodes, EGFR and c-Met protein expression (Fig. 2c) and the proportions of EGFR expression, c-Met expression, both EGFR and c-Met expression, and either expression (EGFR or c-Met) were 68.75%, 62.5%, 43.75%, and 87.5%, respectively (Fig. 2d), indicating that the metastatic lymph nodes had a higher overexpression rate when the two markers were combined than that when expressed alone. The differential expression of EGFR and c-Met in CRC and metastatic lymph nodes indicated a difference in expression between these related tissues. Therefore, analysing the complementarity of c-Met and EGFR expression can significantly improve tumour identification.

Fluorescence characterisation of Rybrevant-IRDye800CW

The spectral properties of the synthesised Rybrevant-IRDye800CW probe were evaluated. The UV-visible-NIR absorption spectra were recorded for Rybrevant, IRDye800CW, Rybrevant-IRDye800CW (Fig. 3a). We analysed the structural formula of Rybrevant, IRDye800CW-NHS and depicted the chemical structure of Rybrevant-IRDye800CW based on the structural formula (Figure S1). The peak of the Rybrevant-IRDye800CW absorption spectrum was 790 nm. The probe had an enhanced absorption peak at 260 nm compared to that of Rybrevant, indicating that IRDye800CW was successfully connected to the Rybrevant antibody. The fluorescence signal of Rybrevant-IRDye800CW appeared between 800 and 1200 nm,

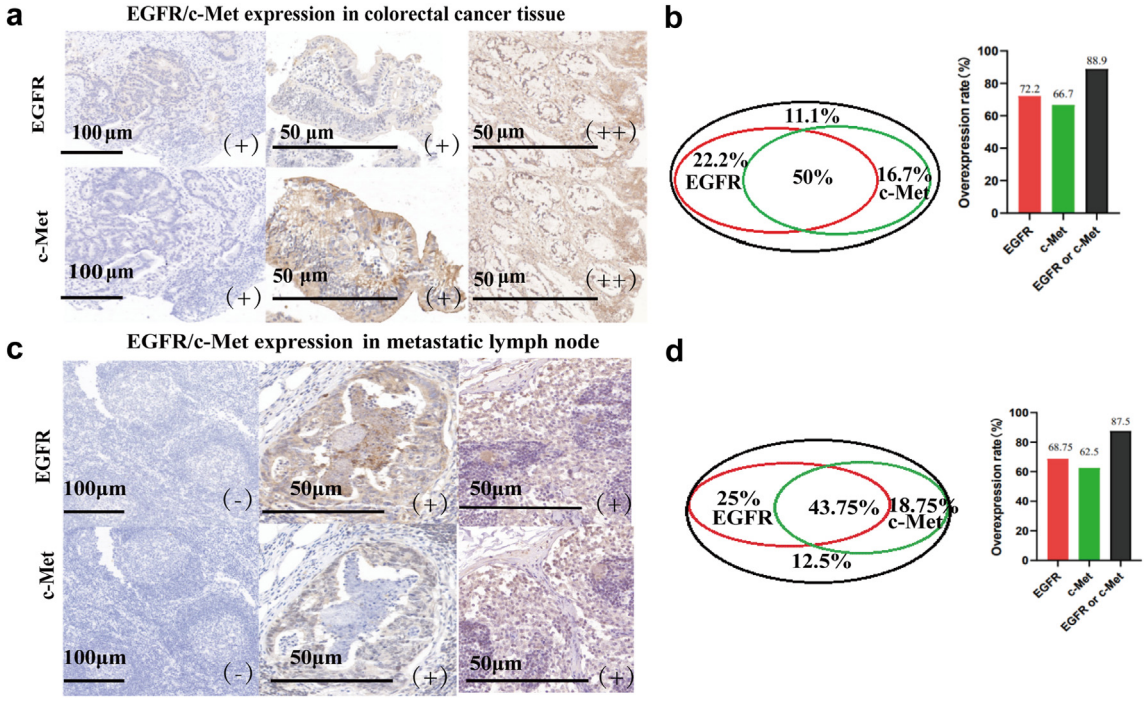

Fig. 2: Expression of EGFR and c-Met in CRC and metastatic lymph nodes. (a) Differential expression of EGFR and c-Met in CRC. (b) Venn diagram showing overexpression ratio of EGFR and c-Met in CRC and their overexpression ratios. (c) Expression of EGFR and c-Met in colorectal metastatic lymph nodes. (d) Venn diagram showing proportion of overexpression of EGFR and c-Met in colorectal metastatic lymph nodes and their overexpression proportions.

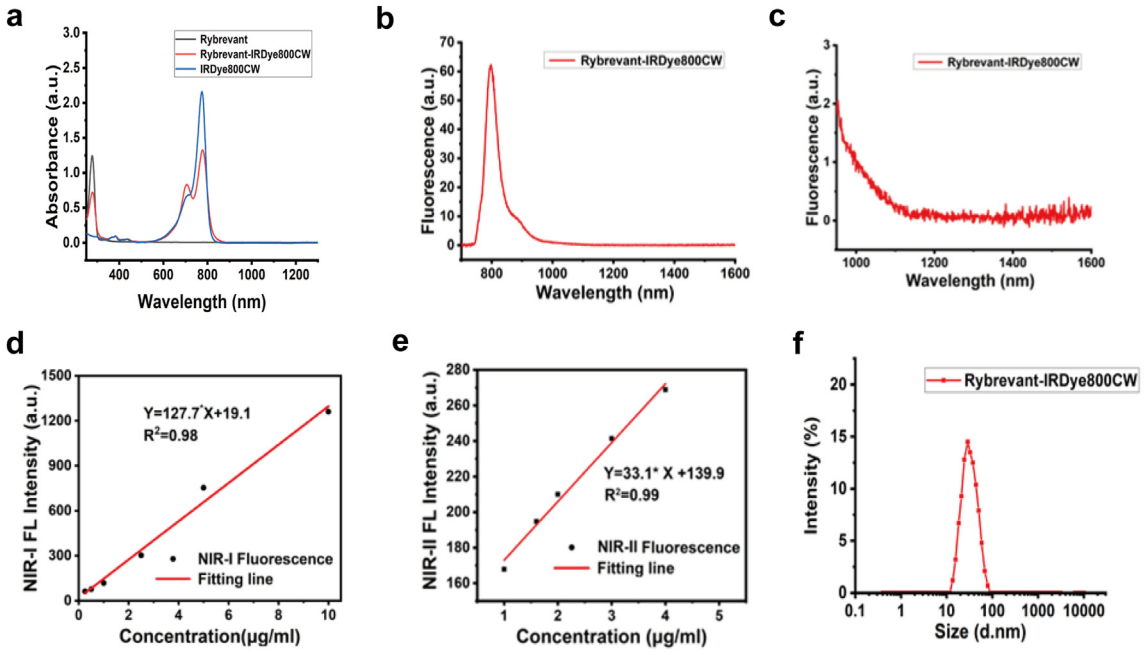

Fig. 3: Characterisation of Rybrevant and Rybrevant-IRDye800CW probes. (a) UV-visible-NIR absorption spectra of Rybrevant, IRDye800CW and Rybrevant-IRDye800CW probe. (b) Fluorescence and (c) emission spectra of Rybrevant-IRDye800CW in NIR-II. Fluorescence signal of probe in (d) NIR-I and (e) NIR-II imaging increased linearly with probe concentration. (f) Hydrated particle size of Rybrevant-IRDye800CW measured using DLS.

and an emission wavelength peak appeared at 818 nm (Fig. 3b and c). Fluorescence imaging of the probe using NIR-I fluorescence showed that the fluorescence signal increased linearly with probe concentration from 0.1 to 10 μg/mL (R2 = 0.98, Fig. 3d). Similarly, the fluorescence signal intensity of the probe in the NIR-II showed a linear enhancement of the fluorescence signal with increasing probe concentration (R2 = 0.99, Fig. 3e). We also detected the hydrodynamic particle size and polydispersity index of the probe by dynamic light scattering (DLS), as shown in Fig. 3f, the hydrated particle size of the probe was 29 nm, and its polydispersity index was 0.26 (Fig. 3f). In order to verify the photostability of Rybrevant-IRDye800CW under laser irradiation, it was continuously irradiated under an excitation laser (1000 nm, 40 W) for 30 min, and the fluorescence intensity of the probe did not weaken with the increase of the laser irradiation time in the above process, which means that there was no photodegradation of Rybrevant-IRDye800CW (Figure S2), indicating that it has excellent photostability. These results indicated that the optical probe Rybrevant-IRDye800CW was successfully synthesised.

Vascular imaging of Rybrevant-IRDye800CW in NIR-II

To test the NIR-II imaging benefits of the Rybrevant-IRDye800CW probe, noninvasive angiography was performed on the left hind limb blood vessels of mice. After the Rybrevant-IRDye800CW probe was injected into the tail vein, NIR-I imaging at 850 nm showed only vaguely shaped blood vessels. By further increasing the wavelength to 1000–1300 nm, clearer vessel shapes were observed with NIR-II imaging (Fig. 4a). Quantitative analysis of the cross-sectional fluorescence intensity distributions of blood vessels showed that when the wavelength was increased from 850 nm to 1300 nm, the NIR-II peak was higher than that of NIR-I (Fig. 4b, white arrows), which suggested that vascular imaging with Rybrevant-IRDye800CW in NIR-II presented a clearer image, especially in regions with fine blood vessels.

EGFR and c-Met expression and Rybrevant-IRDye800CW binding ability in human-derived CRC cell lines *in vitro*

Five human-derived CRC cell lines (SW480, SW620, HCT116, HT29, and RKO) were selected to detect the expression of EGFR and c-Met. Western blotting results showed that EGFR and c-Met were overexpressed in HCT116 and HT29 cell lines, with HCT116 showing the highest expression and RKO showing the lowest expression of EGFR and c-Met (Fig. 5a–c). The results of the protein quantification analysis showed that EGFR was 0.71, 0.61, 0.48, 0.29, and 0.27 in HCT116, HT29 (*p = 0.0317, one-way ANOVA, Fig. 5b), SW620 (**p = 0.0053, one-way ANOVA, Fig. 5b), SW480

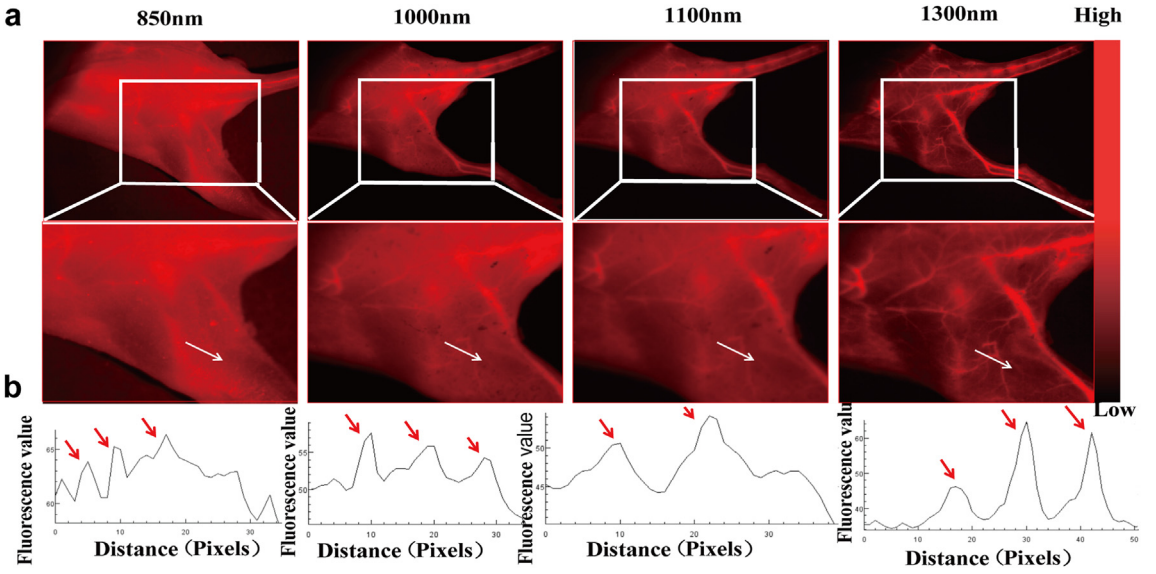

Fig. 4: Rybrevant-IRDye800CW fluorescence using NIR-II vascular imaging. (a) NIR-II images of blood vessels in hind limbs of mice taken with different NIR-II filters on InGaAs camera. Switching to 1300-nm long-pass NIR-II fluorescence greatly improved vascular contrast. (b) Intensity distribution of fluorescence in cross-sections of mouse hind limb vessels in NIR-I and NIR-II windows. Red arrows indicate increasing peaks of fluorescence signal.

(***p = 0.0002, one-way ANOVA, Fig. 5b), and RKO (***p = 0.0001, one-way ANOVA, Fig. 5b) cells, respectively whereas that of c-Met was 0.72, 0.26, 0.36, 0.36, and 0.16 in HCT116, HT29 (**p = 0.0021, one-way ANOVA, Fig. 5d), SW620 (**p = 0.008, one-way ANOVA, Fig. 5d), SW480 (**p = 0.0073, one-way ANOVA, Fig. 5d), and

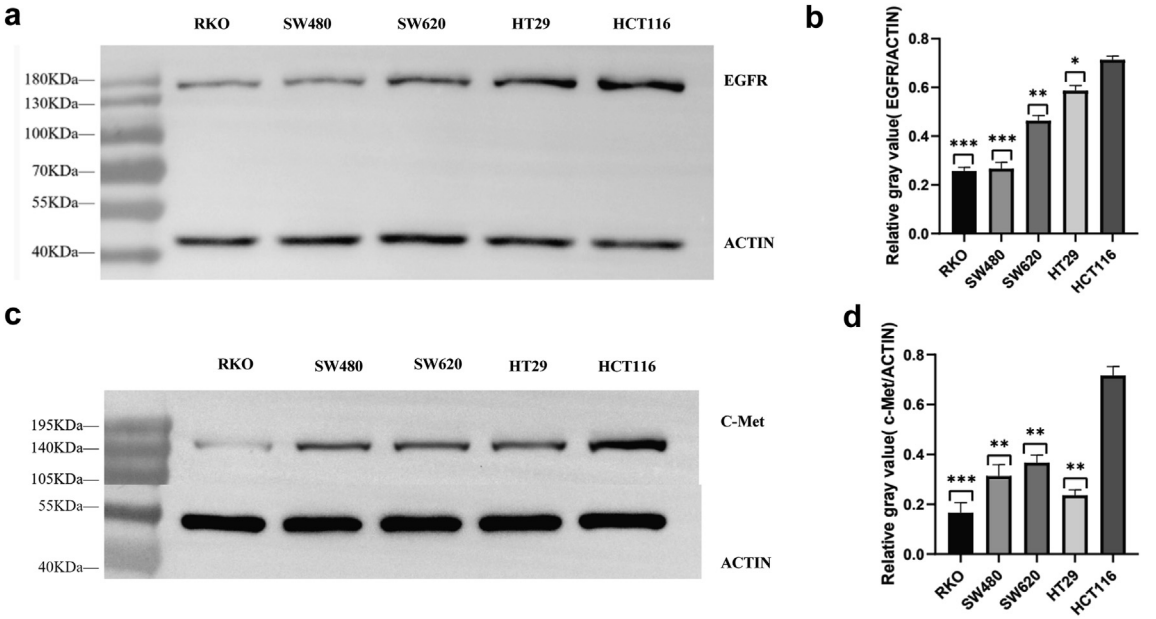

Fig. 5: EGFR and c-Met expression in human-derived CRC cell lines. Western blotting was used to detect (a) EGFR and (c) c-Met expression in human-derived CRC cell lines. (b, d) Western blot results were analysed using ImageJ software. Multiple sets of data were compared and the data satisfied normal distribution and chi-square, using a one-way ANOVA. And the levels of significance were indicated as follows: *p < 0.05, **p < 0.01, ***p < 0.001, and ****p < 0.0001.

RKO (***p = 0.0003, one-way ANOVA, Fig. 5d) cells, respectively. EGFR and c-Met levels were highest in HCT116 cells and lowest in RKO cells (Fig. 5b–d); therefore, we chose HCT116 and RKO cell lines for our study.

To test the targeting ability of the Rybrevant-IRDye800CW probe, we incubated HCT116 and RKO cell lines with 100 nM of the probe for 3 h. Using laser confocal microscopy, we found that the Rybrevant-IRDye800CW probe showed a stronger fluorescence signal in HCT116 cells and a weaker fluorescence signal in RKO cells (Fig. 6a, red fluorescence). Rybrevant-IRDye800CW was localised to the membrane surface of HCT116 cells. The results showed that the probe fluorescence signal intensity in HCT116 cells significantly differed from that in RKO cells (****p < 0.0001, one-way ANOVA, Fig. 6b). To examine probe uptake by HCT116 cells further, we performed target blocking in three additional groups of HCT116 cells. First, we blocked EGFR and c-Met expression by treating HCT116 cells with excess cetuximab and Savolitinib. Since blockade of these receptors by the antibodies decreased the uptake of the Rybrevant-IRDye800CW probe, only weak fluorescence was observed in the two sets of treated HCT116 cells, which was much less than that in the Rybrevant-IRDye800CW group that was not treated with excess antibodies (****p < 0.0001, one-way ANOVA, Fig. 6a). Second, we treated HCT116 cells with excess Savolitinib to block c-Met and observed a decreased uptake of the Rybrevant-IRDye800CW probe. Only weak fluorescence was observed in HCT116 cells when compared to that in the Rybrevant-IRDye800CW control group (****p < 0.0001, one-way ANOVA, Fig. 6a). Quantitative analysis showed that the fluorescence intensity of the blocked group was significantly lower than that of the HT116 unblocked group (Fig. 6b), further suggesting that the dual-target probe had superior binding ability to CRC cells.

In vivo biodistribution of Rybrevant-IRDye800CW probe

Next, we evaluated the *in vivo* biodistribution and tumour selectivity of Rybrevant-IRDye800CW in subcutaneous CRC tumour models. The human CRC cell lines HCT116 and RKO were selected to construct mouse subcutaneous tumours. Two weeks after CRC cell injection, Rybrevant-IRDye800CW was injected into mouse subcutaneous tumours (n = 3) via the tail vein and fluorescence imaging was performed using the NIR-II imaging system to evaluate the specificity of the probes and their biological distribution *in vivo*. The results showed that Rybrevant was mainly metabolised by the liver, and the mouse livers showed strong fluorescent signals, which gradually diminished over time (Fig. 7a). The fluorescent signals started to appear at approximately 6 h, and the fluorescent signal intensity reached the highest value at 24 h (TBR = 2). reached the highest value (TBR = 2.36 ± 0.09). In control RKO subcutaneous tumour-bearing mice (n = 3) injected with the same dose of the probe, the fluorescent signal was weaker and decayed significantly at the tumour with time (TBR = 1.52 ± 0.20, p < 0.001, t-test, Fig. 7b).

In HCT116 tumour-bearing nude mice, we first blocked dual expression of EGFR and c-Met in HCT116 cells with an overdose of Cetuximab and Rybrevant via tail vein injection 24 h before the injection of the probes. Compared with that in the unblocked group, the fluorescence signal was weakened after antibody blockade, and the fluorescence intensity in the Cetuximab group was much lower than that in the Rybrevant-blocked groups, with TBR maxima of 1.77 ± 0.05 and 1.35 ± 0.16, respectively. We also treated the HCT116 cells with an excess of free Savolitinib to block c-Met 24 h before the intravenous injection of the probe and observed only weak fluorescence in the HCT116 cells. This fluorescence was much lower than that in the Rybrevant-IRDye800CW group, and *in vivo* imaging showed a significant decrease in fluorescence signal intensity in the tumour region, with a TBR maximum of 1.77 ± 0.08 (Fig. 7b). Another Rybrevant-IRDye800CW group of mice (n = 3) was euthanised at the optimal imaging time point (24 h) so that the organs and tumours could be dissected. NIR-II imaging was performed on these tissues, which showed that Rybrevant-IRDye800CW was predominantly distributed in the liver and tumour tissues (Fig. 7c and d). Moreover, the Rybrevant-IRDye800CW signal co-localised with EGFR and c-Met markers, further validating its *in vivo* performance (Fig. 7e).

Rybrevant-IRDye800CW in NIR-I and NIR-II fluorescence imaging

We used the HCT116 cell line, constructed a subcutaneous tumour model (n = 3), injected the same Rybrevant-IRDye800CW in the tail vein, and after 24h performed fluorescence imaging in NIR-I and NIR-II respectively and analysed the tumour for fluorescence intensity (Figure S3a), the tumour showed a high fluorescence signal and the NIR-II had a much higher signal-to-back ratio compared NIR-I (Figure S3b).

NIR-II fluorescent surgical navigation guides R0 resection of orthotopic CRC

To evaluate the imaging performance of the dual-specific probe in an orthotopic CRC model further, an orthotopic mouse model of HCT116 human-derived intestinal cancer was established, and orthotopic tumour formation in the caecum was confirmed using bioluminescence imaging (BLI). Rybrevant-IRDye800CW was injected into the tail vein, and the mice were fasted for 24 h. The tumours were then resected under the guidance of white light, NIR-I, and NIR-II fluorescence. When the abdominal cavity was exposed, it was difficult to differentiate the tumour

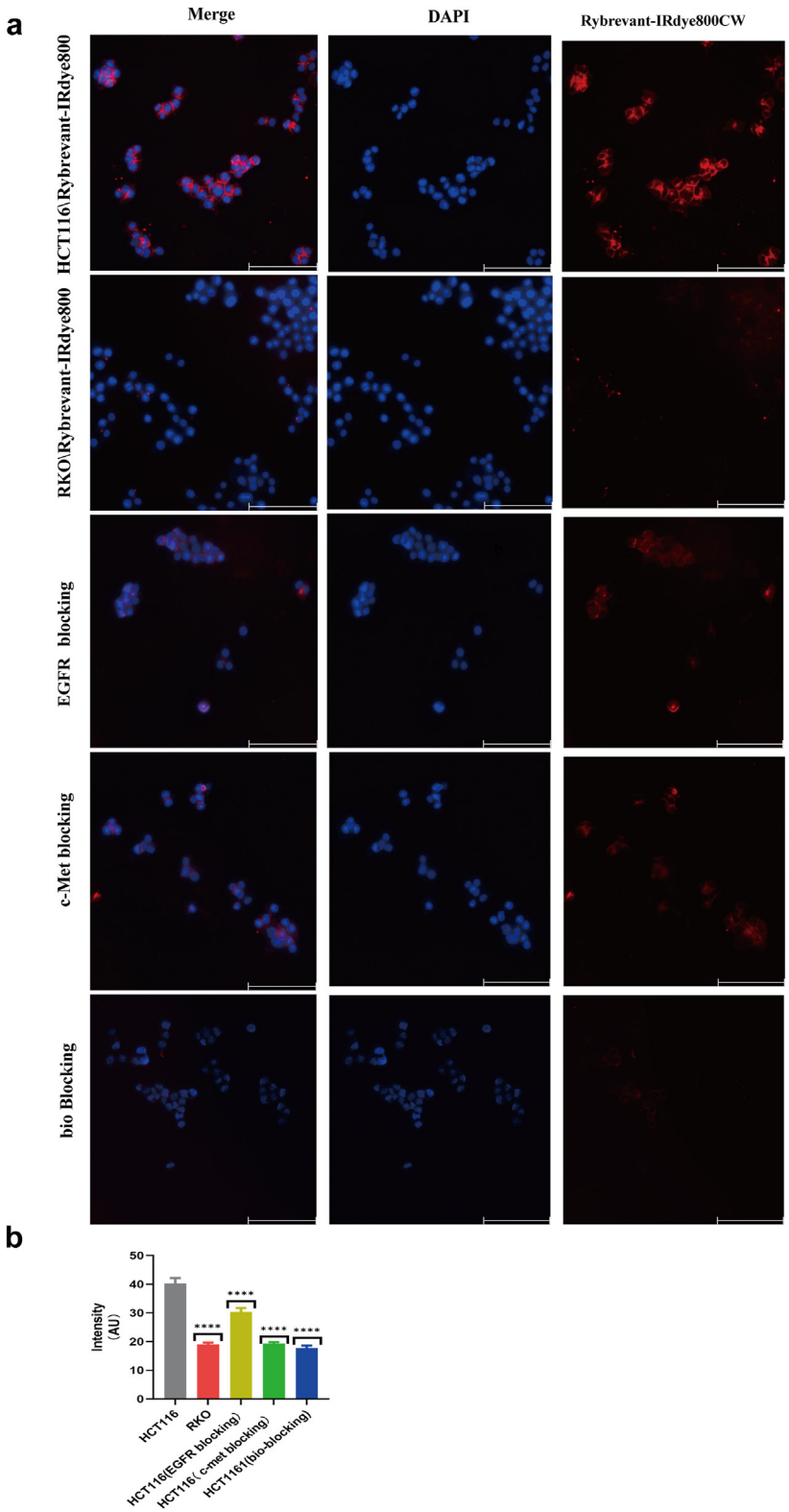

Fig. 6: Assessment of Rybrevant-IRDye800CW *in vitro* targeting. (a) Uptake of Rybrevant-IRDye800CW by different cell subgroups (red) grown under same conditions. Cell nuclei are stained with DAPI (blue). HCT116 cell (EGFR, c-Met; double-positive) uptake of probe was significantly higher than that of RKO cells (low expression of EGFR, c-Met). EGFR, c-Met, and dual blocking of both EGFR and c-Met receptors in

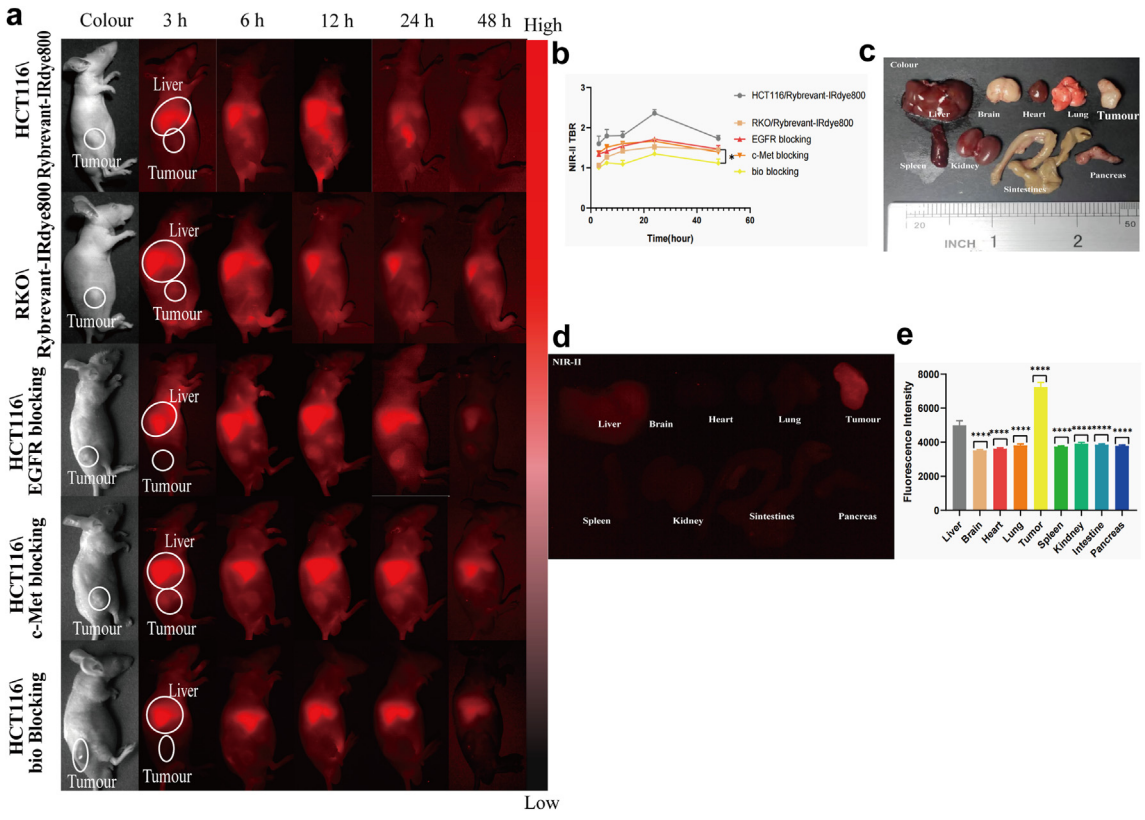

Fig. 7: Specificity and biological distribution of Rybrevant-IRDye800CW *in vivo*. (a) Representative whole-body imaging of HCT116 and RKO subcutaneous xenograft tumour models injected with Rybrevant-IRDye800CW at different time points in (n = 3) and HCT116 subcutaneous tumour EGFR, c-Met, and dual-targeting blockade assays (n = 3). (b) Quantification of Rybrevant-IRDye800CW fluorescence signal intensity in NIR-II and analysis of tumour-to-background ratio. Fluorescence signal intensity of skin around tumour was selected as background (*p < 0.05). (c) Image of organs from mice 24 h after Rybrevant-IRDye800CW in each organ 24 h after intravenous injection in (c) white light and (d) NIR-II. (e) ImageJ software fluorescence quantification was used to analyse fluorescence intensity values of Rybrevant-IRDye800CW in each organ *in vivo*, and statistical analysis (t-test) was considered statistically significant at p < 0.05 (*).

tissue from the surrounding normal tissues under white light; therefore, the nodules were identified in the overlapping area of the combined fluorescence signals from the NIR-I/II imaging and BLI signals for tumour localisation (Fig. 8a–e). The R0 resection of the diseased tissue was performed under NIR-II fluorescence guidance (Fig. 8f). After resection, NIR-II imaging of the original tumour location was performed to confirm that residual high fluorescence signals were present at the tumour location (Fig. 8g), and the resected tumour tissue was observed under white light (Fig. 8h). Subsequent analysis of the difference between NIR-II and NIR-I imaged tumours in five mice demonstrated a significant TBR of NIR-II vs NIR-I (2.55 ± 0.38 vs 1.94 ± 0.20, *p < 0.05, t-test, Fig. 8i). The mice were euthanised and organ dissection was performed to measure the fluorescence signals in the liver and tumour tissues, which were significantly higher than those of other tissues using NIR-II fluorescence imaging; however, the fluorescence signal intensity of the liver was not significantly different from that of tumours (Fig. 8j). The resected tumour tissues were subjected to pathological HE and IHC tests to examine EGFR and c-Met expression (Fig. 8k–n). These results further confirmed the enhanced uptake of the probe by tumours with high EGFR and c-Met expression.

In vivo fluorescence imaging of metastatic lymph nodes in human-derived HCT116 cell model

To evaluate the performance of Rybrevant-IRDye800CW in diagnosing metastatic lymph nodes, a lymph node metastasis mouse model was constructed using

HCT116 cells. (b) Quantitative analysis of probe fluorescence intensity was performed using ImageJ software. Scale bar, 20 μm. Multiple sets of data were compared and the data satisfied normal distribution and chi-square, using a one-way ANOVA. ****p < 0.0001 was regarded as statistically significant.

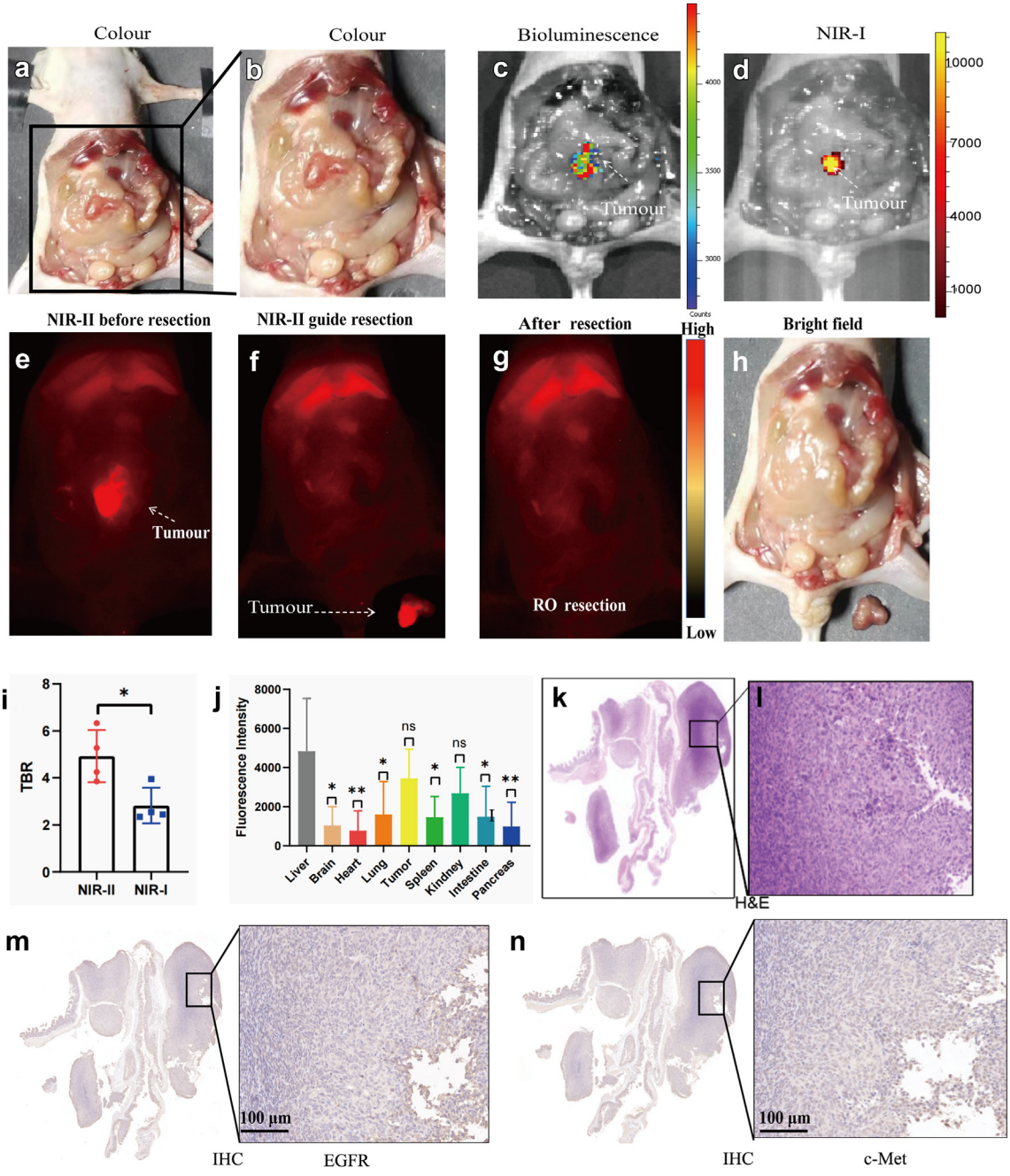

Fig. 8: NIR-II fluorescence-guided R0 resection of colorectal cancer specimen. (a, b) Intraoperative white light, (c) BLI imaging, (d) NIR-I, and (e–g) NIR-II fluorescence imaging of orthotopic tumours (n = 4). (e and f) Tumour sites are indicated using white arrows in NIR-II fluorescence images. (h) White light image of resected tumours. (i) TBR of NIR-I and NIR-II for all tumours (n = 4). (j) Biodistribution of probes *in vivo*. (k, l) HE staining of tumours after resection. (m, n) IHC images of resected tumours. Quantification of fluorescence intensity of tumours was performed, and results were considered statistically significant at $p < 0.05$ (*) using t-test. Scale bar, 100 μm.

HCT116 cells. Human-derived HCT116 tumour cells were injected into the paw pads of mice, and six weeks after inoculation, sentinel metastatic lymph nodes were palpable. The Rybrevant-IRDye800CW probe was injected peri-tumourally into the paw pads, and the lymph nodes were resected under NIR-II imaging guidance. Before resection, the location of the lymph node and its size could not be observed under white light; however, the lymph node fluorescence was stronger, and fine lymphatic vessels were visible under

NIR-II fluorescence imaging (Fig. 9a, yellow arrows). After resection of the lymph node using NIR-II guidance, there was no fluorescence signal in the location of the original lymph node. In contrast, the resected lymph nodes were fluorescent (Fig. 9b, yellow arrows), with a TBR of 2.77 ± 0.56. Moreover, the fluorescent signal intensity of the lymph nodes was higher than that of the surrounding tissues (Fig. 9a and b). After resection, the lymph nodes were observed under white light and NIR-II, which showed that the fluorescent signals under NIR-II were stronger than those under white light (Fig. 9c) and the diameters of the lymph nodes were approximately 4 mm. Pathological HE and IHC staining confirmed the presence of tumour cells and EGFR and c-Met expression in the lymph nodes (Fig. 9d). These results indicated that Rybrevant-IRDye800CW may help the differential diagnosis of metastatic lymph nodes.

Imaging of Rybrevant-IRDye800CW in human CRC fresh specimens

After collecting 24 surgically resected fresh CRC specimens (Table 1), the tumour and lymph node specimens were washed in saline immediately after resection and incubated with Rybrevant-IRDye800CW. NIR-II imaging showed that the fluorescence intensity of the tumour tissue was significantly higher than that of the neighbouring normal intestinal mucosal tissue in the same patient (**p = 0.0039, t-test, Fig. 10a, b, e). The fluorescence intensity of metastatic lymph nodes was significantly higher than that of the normal lymph nodes (*p = 0.0127, t-test, Fig. 10c, d, f). NIR-II imaging of tissues incubated with Rybrevant-IRDye800C revealed that 20 out of 24 tumour tissues and 7 out of 24 pairs of metastatic lymph nodes were EGFR and c-Met positive (Fig. 10g–l).

Discussion

Fluorescence-guided surgery is rapidly entering clinical practice. However, most studies using NIR-I imaging are limited by its imaging resolution and depth, which results in the inability to identify and completely resect tumour tissues and their metastatic lesions.[36] NIR-II (1000–1700 nm) imaging improve the sensitivity and resolution of imaging. Meanwhile in the imaging equipment: the emergence of high sensitivity NIR-II

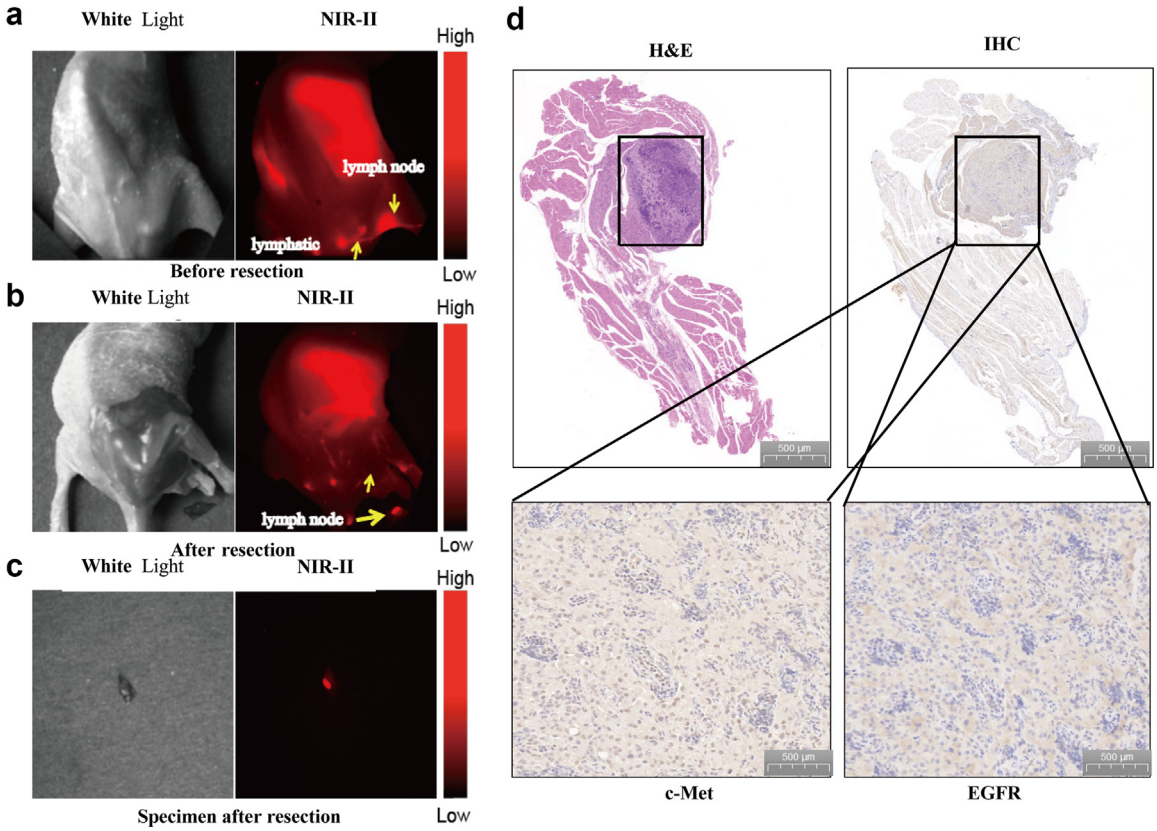

Fig. 9: NIR-II fluorescence-guided lymph node dissection specimens for colorectal cancer. Lymph node and lymphatic vessel imaging under white light and NIR-II fluorescence (a) before and (b) after surgical resection. (c) Diagram showing lymph node specimens after surgical resection in white light and NIR-II fluorescence imaging. (d) HE staining and IHC of lymph nodes after resection.

Characteristic	
Age	
≤60	12 (50%)
≥60	12 (50%)
Sex	
Men	19 (79%)
Women	5 (21%)
Race	Asian: 24 (100%)
Postoperative pathologic staging (AJCC)	
I	3 (12.5%)
II	7 (29%)
III	11 (46%)
IV	3 (12.5%)
Pathologic T-staging	
T0	0
T1	0
T2	4 (17%)
T3	12 (50%)
T4	8 (33%)
Pathologic N-staging	
N0	0
N1	15 (62.5%)
N2	9 (37.5%)
N3	0

We collected 24 colorectal cancer tumour specimens, all of which were surgically excised.

Table 1: **Patient and tumour characteristics.**

camera has improved the imaging speed and depth. The advantages of NIR-II include high resolution: NIR-II has a longer wavelength and less scattering, providing clearer images of deeper tissues. High signal-to-noise ratio: Biological tissues have low autofluorescence in the NIR-II region, resulting in low background noise and high imaging contrast.[37–39] Hu et al. conducted the first clinical study on NIR-II fluorescence-guided hepatic cancer resection, showing its superiority over NIR-I imaging in detecting small liver cancer foci and metastases intraoperatively, significantly enhancing surgical outcomes.[28] Additionally, 2D5-IRDye800CW, an NIR-II fluorescent probe that targets CEACAM5, was designed and synthesised for the precise identification and fluorescence-guided precision resection of CRC and peritoneal metastatic cancer.[32]

To address the heterogeneity of tumour surface receptor expression that leads to poor single-target probe imaging, we constructed the NIR-II probe, Rybrevant-IRDye800CW, in a CRC model that is based on the bispecific antibody Rybrevant for c-Met and EGFR. To our knowledge, this is a study on applying bispecific antibody NIR-II probe imaging for CRC and its metastatic lymph nodes. Rybrevant-IRDye800CW was synthesised by coupling the c-Met and EGFR bispecific antibody Rybrevant with the IRdye800CW dye. We found that the fluorescent signal intensity of Rybrevant-IRDye800CW was stronger *in vitro* cellular uptake assays in highly expressing cell lines and weaker in those expressing lower levels. *In vivo* studies demonstrated that Rybrevant-IRDye800CW had significant tumour enrichment and superior NIR-II (1000 nm–1600 nm) imaging ability, with high resolution and less tissue scattering in subcutaneous CRC tumours overexpressing EGFR and c-Met. Additionally, the probe exhibited good tumour enrichment in an orthotopic CRC tumour model with a significantly higher TBR in both NIR-I and NIR-II ($p = 0.02$). The probe rapidly targeted the tumour area 6 h after tail vein injection and could be used for real-time FGS 6–24 h after injection. Moreover, the tumour retained fluorescence for more than 48 h, which allowed tumour visualisation throughout the entire surgical procedure. The Rybrevant-IRDye800CW probe also showed lymph node visualisation, allowing precise resection in the tumour metastasis lymph node model, and could specifically target EGFR- and c-Met-positive isolated fresh specimens of human CRC. In these cells, the intensity of the Rybrevant-IRDye800CW tumour fluorescence signal was positively correlated with EGFR and c-Met immunohistochemistry results.

Bispecific antibody probes benefit cancer imaging because of the heterogeneity of receptor expression on the tumour surface. This often results in poor or no visualisation of single-target probes.[25,40] Single c-Met or EGFR expression is not high in CRC, and the proportional expression in patients with CRC with dual-target combinations is significantly greater than that of a single target. The EGFR[41] and c-Met[42] receptors are strongly positive in CRC and corresponding metastatic lymph nodes[43]; therefore, it may be appropriate to use them as imaging targets in CRC. The dual-specific probe showed significant tumour-enriched signals in EGFR- and c-Met-overexpressing tumours, suggesting that Rybrevant-IRDye800CW could significantly improve the sensitivity of CRC imaging. This study found that lower MFI and TBR were obtained in EGFR and c-Met double-positive tumour cells after target receptor blockade was administered, and Rybrevant-IRDye800CW had a higher MFI and TBR than the single-target probes.

This study aimed to investigate using probes to support treating more patients with CRC with diverse receptor expression levels. The results of this study showed that the Rybrevant-IRDye800CW probe could identify both EGFR and c-Met double-positive tumours with more clinical application than single-target probes. In addition, our study demonstrated the high uptake of Rybrevant-IRDye800CW by EGFR and c-Met double-positive tumours, which is similar to the results of some preclinical studies on surgical navigation,[28,44] suggesting that Rybrevant-IRDye800CW could be used for surgically navigated resection of CRC.

Detecting metastatic lymph nodes is crucial for colorectal tumour resection because lymph node invasion is associated with poor prognosis in CRC.[8] HCT116

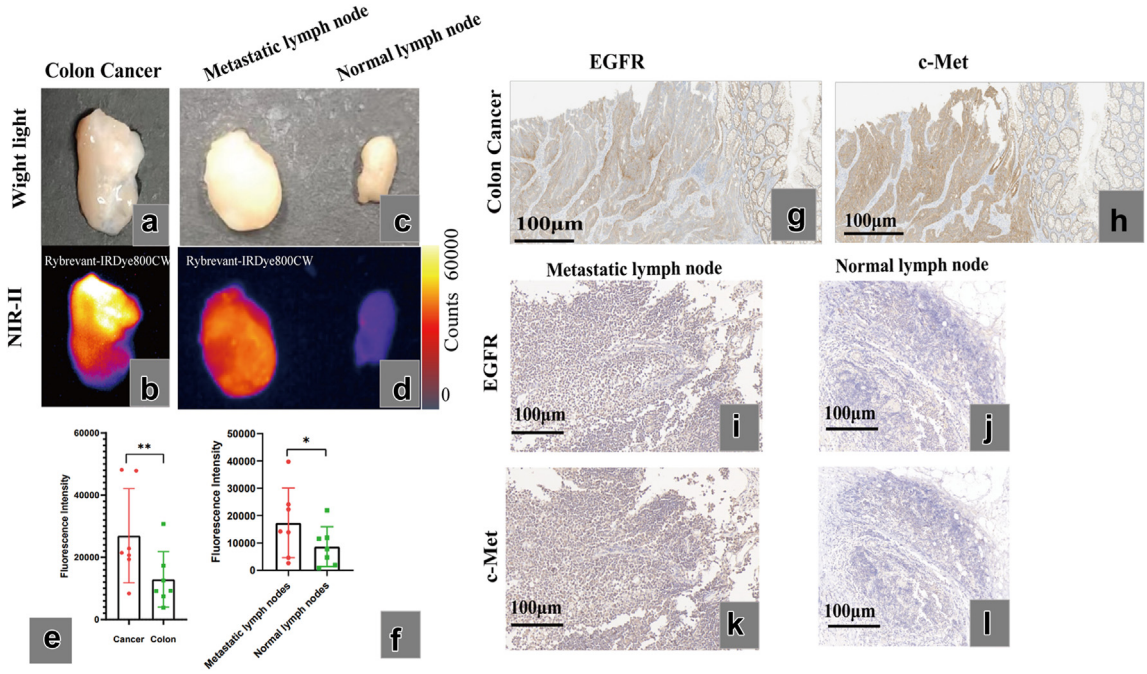

Fig. 10: Human colorectal cancer and lymph node specimens incubated with Rybrevant-IRDye800CW. (a, c) White light images of CRC and normal colorectal tissue and (b, d) their NIR-II images after incubation with Rybrevant-IRDye800CW. Quantification of Rybrevant-IRDye800CW fluorescence intensity in tumour and adjacent intestinal tissues (e) and in metastatic and normal lymph nodes (f). (g, h) IHC staining results of EGFR and c-Met in CRC specimens, respectively. (i) IHC staining results of EGFR in CRC metastatic lymph node specimens. (j) IHC staining results of EGFR in CRC normal lymph node specimens. (k) IHC staining results of c-Met in CRC metastatic lymph node specimens. (l) IHC staining results of c-Met in CRC normal lymph node specimens. Statistical analysis (t-test), $p < 0.05$ (*), $p < 0.01$ (**) was considered statistically significant.

cells were used to construct a cell-derived xenograft lymph node metastasis mouse model to show that the Rybrevant-IRDye800CW probe could identify metastatic lymph nodes. ICG lacks lymph node targeting and cannot identify metastatic lymph nodes, often being found in the non-tumour area of metastatic lymph nodes.[13] The fluorescently labelled anti-human EGFR recombinant antibody scFv fragments incubated with fresh tissues during surgery have a sensitivity of 85.7% and specificity of 100% for identifying lung cancer and a sensitivity of 77.8% and specificity of 92.1% for identifying metastatic lymph nodes.[35] These findings suggest that this technique can be used to identify tumour regions in resected lung tissues rapidly, differentiate between tumour boundaries, and identify lymph node metastasis. Similarly, we found that metastatic lymph nodes were identified after injection of the dual-specific Rybrevant-IRDye800CW probe, and the lymph nodes had strong fluorescence signals. In our lymph node metastasis mouse model, the lymph node was resected under fluorescence guidance and confirmed to contain tumour cells. There was significant expression of c-Met and EGFR in these cells, which may be related to the overexpression of tumour receptors in the metastatic lymph node. These results confirmed that the Rybrevant-IRDye800CW probe can be used to identify CRC metastatic lymph nodes.

Near-infrared fluorescence imaging is a promising technique for improving surgical approaches in the era of precision medicine.[45] Although previous molecular imaging has achieved promising clinical results in tumour imaging, molecular probing, chemiluminescence, and Cherenkov imaging, it has never been possible to perform intraoperative imaging.[38,46–49] The second window of NIR imaging (NIR-II) fluorophores show excellent imaging ability. NIR-II fluorophores, including carbon nanotubes, rare-earth nanoparticles, quantum dots, and organic small molecules, carry some risks in their clinical applications,[50–52] such as biosafety and clinical medical ethics, which require further safety validation. Anthocyanin dyes have an emission peak at 700–900 nm in the NIR-I region; however, its emission tail extends to NIR-II (1000–1700 nm). Therefore, NIR-I dyes such as ICG, IRDye800CW, and IR-12N3 may have additional applications in clinical NIR-II imaging. This study demonstrated the imaging capability of Rybrevant-IRDye800CW at 1000–1300 nm with deeper tissue penetration and higher spatial resolution, facilitating the intraoperative imaging of deeper tissues and fine blood vessels.

Despite the advantages of imaging in this study, there are some limitations, such as the lack of comparison of data such as recurrence rates in subsequent survival of mice and the lack of follow-up of clinical samples with data such as postoperative survival. In addition, CRC surgery is performed clinically using laparoscopic surgery, and our study used an open abdominal imaging approach, due to the fact that the equipment currently available for intraoperative navigation of NIR-II is large open abdominal view imaging. In addition the bispecific fluorescent probes in this study may be limited by the tumour microenvironment in the treatment of solid tumours, such as high mesenchymal pressure and vascular abnormalities, which can impede the effective penetration of drugs. Immunosuppressive factors in the tumour microenvironment may also diminish the efficacy of bispecific probes in tumour therapy. Multiple challenges need to be overcome in clinical development, including optimising the design to increase the therapeutic window, reduce toxicity and improve patient tolerability. This study investigates the value of NIR-II imaging modalities in CRC. Fluorescence endoscopy for NIR-II intraoperative navigation has been developed, which will accelerate the clinical translation of NIR-II. will accelerate the clinical translation of NIR-II.

Rybrevant-IRDye800CW had better tissue penetration and fluorescence signal intensity under NIR-II imaging than those under NIR-I, and it is expected to improve precise tumour resection and the detection of CRC and its metastatic lesions.

Contributors

Study design: Jianqiang Tang, Tian Jie, Zhenhua Hu.
Literature search: Shangkun Jin, Xiaohua Jia.
Data collection: Shangkun Jin, Changjian Li, Xiaohua Jia,
Data analysis: all authors.
Data interpretation: all authors.
Figures: Shangkun Jin, Changjian Li, Xiaohua Jia.
Writing: Shangkun Jin, Changjian Li.
Revise: Shangkun Jin, Xiaohua Jia, Changjian Li.
Access and verification of the data: all authors.
Responsibilities for the decision to submit the manuscript: all authors.

All authors read and approved the final version of the manuscript and ensured that this was the case. All authors reviewed, discussed, and agreed with manuscript submission.

Data sharing statement

The main data supporting the results of this study are available in the paper and its Supplementary Materials. The raw near-infrared fluorescence images can be obtained after asking the corresponding authors and clarifying the purpose of use.

Declaration of interests

The authors declare that they have no conflicts of interest.

Acknowledgements

This study was supported by the Beijing Natural Science Foundation (Grant numbers: L222054, 7244517, 4232058, L248026, L232020), National Natural Science Foundation of China (NSFC) (92059207, 92359301, 92259303, 62027901, 81930053, 81227901, U21A20386), CAS Youth Interdisciplinary Team (JCTD-2021-08), and the Fundamental Research Funds for the Central Universities (Grant no. JK2024-2-35-02).

Appendix A. Supplementary data

Supplementary data related to this article can be found at https://doi.org/10.1016/j.ebiom.2025.105687.

References

1 Sung H, Ferlay J, Siegel RL, et al. Global cancer statistics 2020: GLOBOCAN estimates of incidence and mortality worldwide for 36 cancers in 185 countries. *CA Cancer J Clin*. 2021;71(3):209–249.
2 Siegel RL, Miller KD, Wagle NS, et al. Cancer statistics, 2023. *CA Cancer J Clin*. 2023;73(1):17–48.
3 Cao W, Chen HD, Yu YW, et al. Changing profiles of cancer burden worldwide and in China: a secondary analysis of the global cancer statistics 2020. *Chin Med J*. 2021;134(7):783–791.
4 Miller KD, Nogueira L, Mariotto AB, et al. Cancer treatment and survivorship statistics, 2019. *CA Cancer J Clin*. 2019;69(5):363–385.
5 Amri R, Bordeianou LG, Sylla P, Berger DL. Association of radial margin positivity with colon cancer. *JAMA Surg*. 2015;150(9):890–898.
6 Orosco RK, Tapia VJ, Califano JA, et al. Positive surgical margins in the 10 most common solid cancers. *Sci Rep*. 2018;8(1):5686.
7 Galema HA, Meijer RPJ, Lauwerends LJ, et al. Fluorescence-guided surgery in colorectal cancer; a review on clinical results and future perspectives. *Eur J Surg Oncol*. 2022;48(4):810–821.
8 Kang BM, Park JS, Kim HJ, et al. Prognostic value of mesorectal lymph node Micrometastases in ypN0 rectal cancer after Chemoradiation. *J Surg Res*. 2022;276:314–322.
9 Keller DS, Ishizawa T, Cohen R, Chand M. Indocyanine green fluorescence imaging in colorectal surgery: overview, applications, and future directions. *Lancet Gastroenterol Hepatol*. 2017;2(10):757–766.
10 Zheng S, Zhang Z, Qu Y, et al. Radiopharmaceuticals and fluorescein sodium mediated triple-modality molecular imaging allows precise image-guided tumor surgery. *Adv Sci*. 2019;6(13):1900159.
11 Zhang Z, He K, Chi C, et al. Intraoperative fluorescence molecular imaging accelerates the coming of precision surgery in China. *Eur J Nucl Med Mol Imaging*. 2022;49(8):2531–2543.
12 Mieog JSD, Achterberg FB, Zlitni A, et al. Fundamentals and developments in fluorescence-guided cancer surgery. *Nat Rev Clin Oncol*. 2022;19(1):9–22.
13 Sato Y, Satoyoshi T, Okita K, et al. Snapshots of lymphatic pathways in colorectal cancer surgery using near-infrared fluorescence, in vivo and ex vivo. *Eur J Surg Oncol*. 2021;47(12):3130–3136.
14 Turker NS, Heidari P, Kucherlapati R, et al. An EGFR targeted PET imaging probe for the detection of colonic adenocarcinomas in the setting of colitis. *Theranostics*. 2014;4(9):893–903.
15 Diagaradjane P, Orenstein-Cardona JM, Colón-Casasnovas NE, et al. Imaging epidermal growth factor receptor expression in vivo: pharmacokinetic and biodistribution characterisation of a bioconjugated quantum dot nanoprobe. *Clin Cancer Res*. 2008;14(3):731–741.
16 Burggraaf J, Kamerling IM, Gordon PB, et al. Detection of colorectal polyps in humans using an intravenously administered fluorescent peptide targeted against c-Met. *Nat Med*. 2015;21(8):955–961.
17 de Jongh SJ, Vrouwe JPM, Voskuil FJ, et al. The optimal imaging window for dysplastic colorectal polyp detection using c-met-targeted fluorescence molecular endoscopy. *J Nucl Med*. 2020;61(10):1435–1441.
18 de Jongh SJ, Voskuil FJ, Schmidt I, et al. c-Met targeted fluorescence molecular endoscopy in Barrett's esophagus patients and identification of outcome parameters for phase-I studies. *Theranostics*. 2020;10(12):5357–5367.
19 Kang J, Sun T, Zhang Y. Immunotherapeutic progress and application of bispecific antibody in cancer. *Front Immunol*. 2022;13:1020003.
20 Galizia G, Lieto E, De Vita F, et al. Cetuximab, a chimeric human mouse anti-epidermal growth factor receptor monoclonal antibody, in the treatment of human colorectal cancer. *Oncogene*. 2007;26:3654–3660.
21 Ciardiello F, Tortora G. EGFR antagonists in cancer treatment. *N Engl J Med*. 2008;358(11):1160–1174.

22 Kammula US, Kuntz EJ, Francone TD, et al. Molecular co-expression of the c-Met oncogene and hepatocyte growth factor in primary colon cancer predicts tumour stage and clinical outcome. *Cancer Lett*. 2007;248(2):219–228.
23 Di Renzo MF, Olivero M, Giacomini A, et al. Overexpression and amplification of the met/HGF receptor gene during the progression of colorectal cancer. *Clin Cancer Res*. 1995;1(2):147–154.
24 El-Deiry WS, Vijayvergia N, Xiu J, et al. Molecular profiling of 6,892 colorectal cancer samples suggests different possible treatment options specific to metastatic sites. *Cancer Biol Ther*. 2015;16(12):1726–1737.
25 Cavaliere A, Sun S, Lee S, et al. Development of [89Zr]ZrDFO-Amivantamab bispecific to EGFR and c-Met for PET imaging of triple-negative breast cancer. *Eur J Nucl Med Mol Imaging*. 2021;48(2):383–394.
26 Shim H. Bispecific antibodies and antibody-drug conjugates for cancer therapy: technological considerations. *Biomolecules*. 2020;10(3):360.
27 Cho BC, Simi A, Sabari J, et al. Amivantamab, an Epidermal Growth Factor Receptor (EGFR) and mesenchymal-epithelial transition factor (MET) bispecific antibody, designed to enable multiple mechanisms of action and broad clinical applications. *Clin Lung Cancer*. 2023;24(2):89–97.
28 Hu Z, Fang C, Li B, et al. First-in-human liver-tumour surgery guided by multispectral fluorescence imaging in the visible and near-infrared-I/II windows. *Nat Biomed Eng*. 2020;4(3):259–271.
29 Safiejko K, Tarkowski R, Kozlowski TP, et al. Safety and efficacy of indocyanine green in colorectal cancer surgery: a systematic review and meta-analysis of 11,047 patients. *Cancers*. 2022;14(4):1036.
30 Cao C, Deng S, Wang B, et al. Intraoperative near-infrared II window fluorescence imaging-assisted nephron-sparing surgery for complete resection of cystic renal masses. *Clin Transl Med*. 2021;11(10):e604.
31 Cao C, Jin Z, Shi X, et al. First clinical investigation of near-infrared window IIa/IIb fluorescence imaging for precise surgical resection of gliomas. *IEEE Trans Biomed Eng*. 2022;69(8):2404–2413.
32 Guo X, Li C, Jia X, et al. NIR-II fluorescence imaging-guided colorectal cancer surgery targeting CEACAM5 by a nanobody. *eBioMedicine*. 2023;89:104476.
33 Rosenthal EL, Moore LS, Tipirneni K, et al. Sensitivity and specificity of Cetuximab-IRDye800CW to identify regional metastatic disease in head and neck cancer. *Clin Cancer Res*. 2017;23(16):4744–4752.
34 Gao RW, Teraphongphom N, de Boer E, et al. Safety of panitumumab-IRDye800CW and cetuximab-IRDye800CW for fluorescence-guided surgical navigation in head and neck cancers. *Theranostics*. 2018;8(9):2488–2495.
35 Li C, Mi J, Wang Y, et al. New and effective EGFR-targeted fluorescence imaging technology for intraoperative rapid determination of lung cancer in freshly isolated tissue. *Eur J Nucl Med Mol Imaging*. 2023;50(2):494–507.
36 Hernot S, van Manen L, Debie P, et al. Latest developments in molecular tracers for fluorescence image-guided cancer surgery. *Lancet Oncol*. 2019;20(7):e354–e367.
37 He S, Song J, Qu J, Cheng Z. Crucial breakthrough of second near-infrared biological window fluorophores: design and synthesis toward multimodal imaging and theranostics. *Chem Soc Rev*. 2018;47(12):4258–4278.
38 Hu Z, Chen WH, Tian J, Cheng Z. NIRF nanoprobes for cancer molecular imaging: approaching clinic. *Trends Mol Med*. 2020;26(5):469–482.
39 Wang B, Tang C, Lin E, et al. NIR-II fluorescence-guided liver cancer surgery by a small molecular HDAC6 targeting probe. *eBioMedicine*. 2023;98:104880.
40 Liang M, Wang L, Xiao Y, et al. Preclinical evaluation of a novel EGFR&c-Met bispecific near infrared probe for visualisation of esophageal cancer and metastatic lymph nodes. *Eur J Nucl Med Mol Imaging*. 2023;50(9):2787–2801.
41 McKay JA, Murray LJ, Curran S, et al. Evaluation of the epidermal growth factor receptor (EGFR) in colorectal tumours and lymph node metastases. *Eur J Cancer*. 2002;38(17):2258–2264.
42 Takeuchi H, Bilchik A, Saha S, et al. c-Met expression level in primary colon cancer: a predictor of tumour invasion and lymph node metastases. *Clin Cancer Res*. 2003;9(4):1480–1488.
43 Ye P, Li F, Wei Y, et al. EGFR, HER2, and HER3 protein expression in paired primary tumour and lymph node metastasis of colorectal cancer. *Sci Rep*. 2022;12(1):2894.
44 Rosenthal EL, Warram JM, de Boer E, et al. Safety and tumour specifcity of cetuximab-IRDye800 for surgical navigation in head and neck cancer. *Clin Cancer Res*. 2015;21(16):3658–3666.
45 Zhang Z, Du Y, Shi X, et al. NIR-II light in clinical oncology: opportunities and challenges. *Nat Rev Clin Oncol*. 2024;21(6):449–467.
46 Cai M, Zhang Z, Shi X, Yang J, Hu Z, Tian J. Non-negative iterative convex refinement approach for accurate and robust reconstruction in Cerenkov luminescence tomography. *IEEE Trans Med Imaging*. 2020;39(10):3207–3217.
47 Ding X, Wang K, Jie B, Luo Y, Hu Z, Tian J. Probability method for Cerenkov luminescence tomography based on conformance error minimisation. *Biomed Opt Express*. 2014;5(7):2091–2112.
48 Qin C, Zhong J, Hu Z, et al. Recent advances in Cerenkov luminescence and tomography imaging. *IEEE J Sel Top Quantum Electron*. 2011;18(3):1084–1093.
49 Zhang Q, Zhao H, Chen D, et al. Source sparsity based primal-dual interior-point method for three-dimensional bioluminescence tomography. *Opt Commun*. 2011;284(24):5871–5876.
50 Chang B, Li D, Ren Y, et al. A phosphorescent probe for in vivo imaging in the second near-infrared window. *Nat Biomed Eng*. 2022;6(5):629–639.
51 Qu Q, Zhang Z, Guo X, et al. Novel multifunctional NIR-II aggregation-induced emission nanoparticles-assisted intraoperative identification and elimination of residual tumour. *J Nanobiotechnology*. 2022;20(1):143.
52 Yang J, He S, Hu Z, et al. In vivo multifunctional fluorescence imaging using liposome-coated lanthanide nanoparticles in near-infrared-II/IIa/IIb windows. *Nano Today*. 2021;38:101120.